

A SPITZER SPACE TELESCOPE STUDY OF SN 2003gd: STILL NO DIRECT EVIDENCE THAT CORE-COLLAPSE SUPERNOVAE ARE MAJOR DUST FACTORIES

W. P. S. MEIKLE,¹ S. MATTILA,² A. PASTORELLO,² C. L. GERARDY,¹ R. KOTAK,² J. SOLLERMAN,³ S. D. VAN DYK,⁴
D. FARRAH,⁵ A. V. FILIPPENKO,⁶ P. HÖFLICH,⁷ P. LUNDQVIST,⁸ M. POZZO,⁹ AND J. C. WHEELER¹⁰

Received 2007 February 27; accepted 2007 May 9

ABSTRACT

We present a new, detailed analysis of late-time mid-infrared observations of the Type II-P supernova (SN) 2003gd. At about 16 months after the explosion, the mid-IR flux is consistent with emission from $4 \times 10^{-5} M_{\odot}$ of newly condensed dust in the ejecta. At 22 months emission from pointlike sources close to the SN position was detected at 8 and 24 μm . By 42 months the 24 μm flux had faded. Considerations of luminosity and source size rule out the ejecta of SN 2003gd as the main origin of the emission at 22 months. A possible alternative explanation for the emission at this later epoch is an IR echo from preexisting circumstellar or interstellar dust. We conclude that, contrary to the claim of Sugerman and coworkers, the mid-IR emission from SN 2003gd does not support the presence of $0.02 M_{\odot}$ of newly formed dust in the ejecta. There is, as yet, no direct evidence that core-collapse supernovae are major dust factories.

Subject headings: supernovae: general — supernovae: individual (SN 2003gd)

Online material: color figure

1. INTRODUCTION

Massive stars explode via core collapse and ejection of their surrounding layers (e.g., Arnett et al. 1989 and references therein). The extent to which core-collapse supernovae (CCSNe) are, or have been, a major source of dust in the universe is of great interest. For many years it has been hypothesized that the physical conditions in the expanding ejecta of CCSNe could result in the condensation of large masses of dust grains (Cernuschi et al. 1967; Hoyle & Wickramasinghe 1970; Gehrz 1989; Tielens 1990; Dwek 1998; Todini & Ferrara 2001; Nozawa et al. 2003). This follows from the fact that large abundances of suitable refractory elements are present. In addition, cooling by adiabatic expansion and molecular emission takes place, and dynamical instabilities can produce density enhancements or “clumping.” This, in turn, will aid dust formation through the effects of cooling and self-shielding. Further support for these ideas is provided by isotopic anomalies in meteorites, which indicate that some grains must have formed in CCSNe (Clayton et al. 1997).

Interest in CCSNe as dust producers has increased recently due to the problem of accounting for the presence of dust at high redshifts (Fall et al. 1989, 1996; Pei et al. 1991; Pettini et al. 1997; Bertoldi et al. 2003). In these early eras, much less dust production from novae and asymptotic giant branch stars is expected since fewer stars will have evolved past the main-sequence phase. Consequently, CCSNe arising from Population III stars have been proposed as the main early-universe source of dust (Todini & Ferrara 2001; Nozawa et al. 2003). Models of dust formation in CCSNe (Todini & Ferrara 2001; Nozawa et al. 2003) succeed in producing copious amounts of dust—around 0.1 – $1 M_{\odot}$ even in the low-metallicity environments at high redshifts. This corresponds to a supernova (SN) dust condensation efficiency of about 0.2 (Morgan & Edmunds 2003), where the efficiency is defined as the dust mass divided by the total mass of refractory elements. This is enough to account for the quantity of dust seen at high redshifts (see Appendix).

Newly condensed dust in CCSNe can be detected by its attenuating effects on optical/near-IR light or via thermal emission from the grains in the ejecta. These methods have been used in attempts to measure the dust productivity of CCSNe. Both methods are subject to uncertainties due to dust formation in optically thick clumps, so the derived masses tend to be just lower limits. By far the most extensive evidence for ejecta dust condensation is that obtained from the peculiar Type II SN 1987A, where both techniques were employed (Danziger et al. 1989; Lucy et al. 1989; Meikle et al. 1989; Whitelock et al. 1989; Suntzeff & Bouchet 1990; Dwek et al. 1992; Roche et al. 1993; Wooden et al. 1993; Ercolano et al. 2007). However, even the highest value obtained is only $7.5 \times 10^{-4} M_{\odot}$ (Ercolano et al. 2007). Pozzo et al. (2004) used the attenuation method to infer a dust mass exceeding $2 \times 10^{-3} M_{\odot}$ in the Type II SN 1998S. However, such events are relatively rare. Moreover, in this case it is suggested that the dust condensation was not in the body of the ejecta, but rather took place in the cool, dense shell produced by the impact of the SN ejecta with circumstellar material (CSM). We note also that an alternative IR-echo scenario for SN 1998S is not ruled out (Gerardy et al. 2002; Pozzo et al. 2004).

¹ Astrophysics Group, Blackett Laboratory, Imperial College London, London SW7 2AZ, UK; p.meikle@imperial.ac.uk, c.gerardy@imperial.ac.uk.

² Astrophysics Research Centre, School of Mathematics and Physics, Queen’s University Belfast, BT7 1NN, UK; s.mattila@qub.ac.uk, a.pastorello@qub.ac.uk, r.kotak@qub.ac.uk.

³ Dark Cosmology Centre, Niels Bohr Institute, University of Copenhagen, Juliane Maries Vej 30, 2100 Copenhagen, Denmark; jesper@astro.su.se.

⁴ *Spitzer* Science Center/Caltech, Pasadena, CA 91125; vandyk@ipac.caltech.edu.

⁵ Department of Astronomy, Cornell University, Ithaca, NY 14853; duncan@isc.astro.cornell.edu.

⁶ Department of Astronomy, University of California, Berkeley, CA 94720-3411; alex@astro.berkeley.edu.

⁷ Department of Physics, Florida State University, Tallahassee, FL 32306; pah@astro.physics.fsu.edu.

⁸ Stockholm University, AlbaNova University Center, Stockholm Observatory, Department of Astronomy, SE-106 91 Stockholm, Sweden; peter@astro.su.se.

⁹ Department of Earth Sciences, University College London, London WC1E 6BT, UK; m.pozzo@ucl.ac.uk.

¹⁰ University of Texas, Department of Astronomy, Austin, TX 78712; wheel@astro.as.utexas.edu.

Prior to the launch of the *Spitzer Space Telescope* (hereafter, *Spitzer*), the only evidence of dust condensation in a typical CCSN was presented by Elmhamdi et al. (2003), who used optical line attenuation to infer a dust mass lower limit of about $10^{-4} M_{\odot}$ in the Type II-plateau (II-P) SN 1999em. Mid-IR studies of the Cassiopeia A supernova remnant (SNR) (Dwek et al. 1987; Lagage et al. 1996; Douvion et al. 2001) indicate that dust formation took place during its explosion, but again the mass of directly observed dust is small. Submillimeter studies of this SNR by Dunne et al. (2003) using SCUBA led them to claim that at least $2 M_{\odot}$ of dust formed in the supernova. However, Krause et al. (2004) have used the same data together with observations from *Spitzer* to show that most of this emission originates from a line-of-sight molecular cloud, and not from dust formed in Cas A. Temim et al. (2006) used *Spitzer* observations to estimate 10^{-3} to $10^{-2} M_{\odot}$ of dust in the Crab Nebula SNR. While rather uncertain, this result may be more relevant to this paper than that of Cas A, since the Crab Nebula is thought to have arisen from a progenitor of mass 8–10 M_{\odot} (Nomoto et al. 1982; Kitaura et al. 2006), similar to that of the CCSN studied here (SN 2003gd).

In summary, prior to the launch of *Spitzer*, direct observations of CCSNe or SNRs have never revealed more than $\sim 10^{-3} M_{\odot}$ of dust—only $\sim 1\%$ of the mass required if CCSNe are to be important dust sources. But the number of CCSNe investigated for dust production is small, and with the exception of SN 1999em, rather atypical. The availability of *Spitzer* has provided an excellent opportunity for us to test the ubiquity of dust condensation in a statistically significant number of typical CCSNe. It provides high-sensitivity imaging over the mid-IR, covering the likely peak of the dust thermal emission spectrum. This can provide a superior measure of the total flux, temperature and, possibly, dust emissivity than can be achieved at shorter wavelengths. Moreover, the longer wavelength coverage of *Spitzer* lets us detect cooler grains and see more deeply into dust clumps than was previously possible for typical nearby CCSNe. In addition, multiepoch observations with *Spitzer* can distinguish between dust condensation and IR echoes via the strength and shape of the light curve.

In this paper we analyze *Spitzer* observations of the Type II-P SN 2003gd at three late-time epochs. Hendry et al. (2005) and Sugerman et al. (2006) (hereafter S06) reported optical attenuation effects in the late-time spectra and *BR* light curves of SN 2003gd that indicate dust condensation in this event. Using *Spitzer* observations at two late-time epochs, S06 also report mid-IR emission from the condensing dust. This was the first-ever report of condensing dust in a SN II-P on the basis of thermal emission from the grains. Here we present a new study of these *Spitzer* observations. We agree with S06 that some of the earlier epoch mid-IR emission was due to a modest quantity of ejecta dust. However, we find that their principal conclusion, that the later epoch observations indicate the presence of $0.02 M_{\odot}$ of dust formed in the ejecta, is not supported by the data. Consequently, thus far there is no direct evidence that CCSNe are major dust factories.

2. OBSERVATIONS

SN 2003gd was discovered (Evans & McNaught 2003) on 2003 June 12 (UT dates are used throughout this paper) in the SA(s)c galaxy NGC 628 (M74). On 2003 June 13 it was identified as a Type II event (Garnavich & Bass 2003) using a *J*-band spectrum. On 2003 June 14 the identification was confirmed using optical spectra, and it was estimated that the SN was roughly 1 month (Phillips et al. 2003) or 2 months (Kotak et al. 2003) post-explosion at the time of discovery. Using light-curve comparison with other SNe II-P, it was deduced (Van Dyk et al. 2003; Hendry et al. 2005) that SN 2003gd was a normal Type II-P event with

estimated explosion dates of, respectively, 2003 March 17 ± 3 (Van Dyk et al. 2003) or 18 ± 21 (Hendry et al. 2005). We adopt 2003 March 17 as the explosion date, 87 days predisccovery.

On the basis of a variety of methods (standardized candle method, brightest supergiants, kinematic) a distance to SN 2003gd of 9.3 ± 1.8 Mpc was found (Hendry et al. 2005). Modeling of the light echo of SN 2003gd (Van Dyk et al. 2006) suggests a somewhat smaller distance of about 7 Mpc. S06 adopted 9.3 Mpc, and so for ease of comparison with their work we shall adopt 9.3 Mpc throughout. Total extinction (Galactic + host galaxy) estimates of $E(B - V) = 0.13 \pm 0.03$ mag (Van Dyk et al. 2003) and $E(B - V) = 0.14 \pm 0.06$ mag (Hendry et al. 2005) were reported. Using two independent methods (bolometric luminosity of exponential tail; direct comparison with SN 1987A bolometric light curve), Hendry et al. estimate an ejected ^{56}Ni mass of $0.016_{-0.006}^{+0.010} M_{\odot}$, only about a fifth of the ^{56}Ni mass found in SN 1987A (Whitelock et al. 1988; Bouchet et al. 1991). The progenitor star was identified in archival images from the *Hubble Space Telescope*, the 2.6 m Nordic Optical Telescope, and Gemini North, as a red supergiant of mass 6–12 M_{\odot} (Van Dyk et al. 2003; Smartt et al. 2004).

The field of SN 2003gd was observed with *Spitzer*'s Infrared Array Camera (IRAC) at 3.6, 4.5, 5.8, and 8.0 μm on 2004 July 25 and 28 (days 496 and 499) and again on 2005 January 15 (day 670). The first two SN observations were obtained serendipitously within the *Spitzer* Infrared Nearby Galaxies Survey (SINGS) (PID: 0159; Kennicutt et al. 2003). In the SINGS program observations are duplicated with a delay of a few days, to permit identification of asteroids and to better sample the emission on subpixel scales (Regan et al. 2004). In each wavelength channel the two images are combined to yield an “enhanced data product,” and these are publicly available from the NED database. The 2005 January observation was obtained within our *Spitzer* supernova program (PID: 3248). The SINGS program also used the Multiband Imaging Spectrometer for *Spitzer* (MIPS) to acquire images of the field of SN 2003gd at 24 μm on 2005 January 23 and 26 (days 678 and 681). In our measurement and analysis of the days 496 and 499, 670, and 678 and 681 observations, we used the same data as were available to S06. SN 2003gd was again observed at 24 μm within the *Spitzer* supernova program of Sugerman et al. (PID: 30494) on 2006 September 1 (day 1264). Subsequent to the initial submission of this paper, B. Sugerman kindly made this image available to us. We therefore also consider the implications of this observation.

3. RESULTS

A point source at the SN position is clearly visible in the days 496 and 499 image in all four IRAC channels, with strong fading by day 670. This is illustrated in Figures 1a and 1b, where we show the 8 μm IRAC images from days 496 and 499 and day 670. Given the large decline in flux, we deduce that most of the point-source flux detected on days 496 and 499 was due to the SN. However, measurement of the SN flux is challenging owing to the bright, complex field within which it lies.

3.1. Days 496 and 499 Results

3.1.1. PSF-Fitting Measurements

We used the SNOOPY point-spread function (PSF) fitting package to determine the SN fluxes and coordinates. SNOOPY was originally designed by F. Patat to carry out SN photometry. It was implemented in IRAF by E. Cappellaro and is based on DAOPHOT, and has been tested and improved over a number of years. Several suitable PSF stars are selected in order to build the

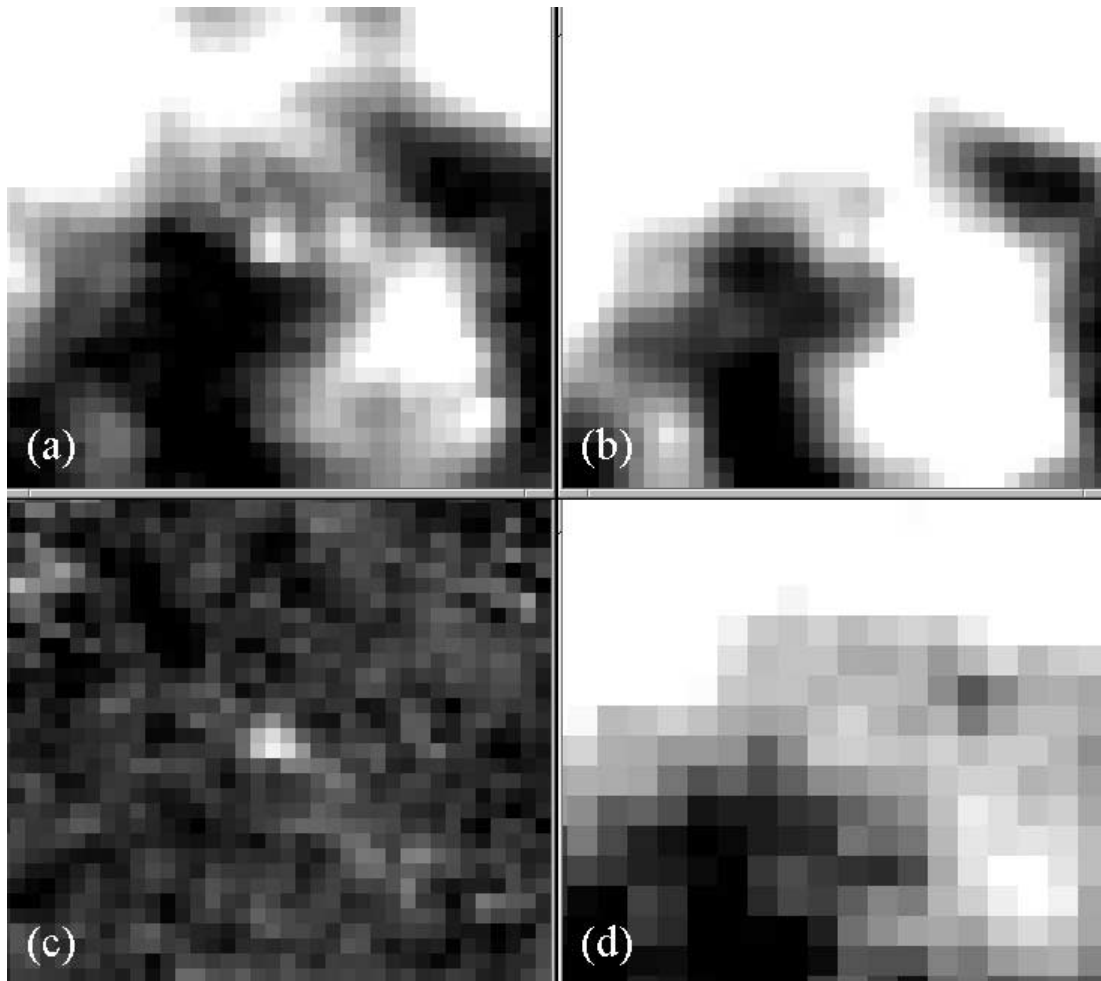


FIG. 1.—Panels *a* and *b* show the field of SN 2003gd at $8\ \mu\text{m}$ (IRAC) on days 496 and 499 and day 670, respectively. Panel *c* shows the result of subtracting (*b*) from (*a*). The bright point source is SN 2003gd. Panel *d* shows the field of SN 2003gd at $24\ \mu\text{m}$ (MIPS) on days 678–681. North is up, and east is to the left. The pixel scales are $0.75''$ and $1.5''\ \text{pixel}^{-1}$ at 8 and $24\ \mu\text{m}$, respectively. Each panel is centered on the supernova position, determined using PSF fitting and the IRAF GEOMAP package (see text).

model PSF and measure the FWHM. First a polynomial surface, of orders between 3 and 6 in x and y , is fitted to the background in a $(10 \times \text{FWHM}) \times (10 \times \text{FWHM})$ region centered on the SN position, excluding the innermost square region around the SN, of side $\sim 1.5 \times \text{FWHM}$. This is then subtracted from the image. Next the PSF fitting is performed on the SN. The fitted PSF is subsequently subtracted from the data to produce a residual image. This is inspected by eye, and the fitting procedure repeated until a residual image is obtained where there is little sign of the original point source. The code returns the x and y position and the flux within the PSF. It also provides a statistical uncertainty, which is a measure of how well the model PSF describes the flux value and distribution at the SN position. However, the flux values are quite sensitive to the fitting of the image background with the polynomial surface. This may introduce an additional uncertainty in the absolute flux values, although the effect on the shape of the spectral energy distribution is likely to be less than this.

The results and estimated uncertainties are shown in Table 1. As a check of the PSF-fitting procedure, field stars were also measured using both this method and aperture photometry. The aperture radius was $10''$ with a 15 – $20''$ concentric sky annulus. No significant systematic flux difference was found between the two methods at any wavelength. The rms scatter in the differences was 0.05 – 0.18 mag. The rms scatter at each wavelength was

adopted as the uncertainty. As a further check, we performed aperture photometry for three stars in both postbasic calibrated data (PBCD) and SINGS-processed IRAC $8\ \mu\text{m}$ frames, and found that the photometry agrees to within 5%. This test was also applied to the days 678–681 MIPS $24\ \mu\text{m}$ frames (see below) and similar consistency was obtained.

3.1.2. Image Subtraction Measurements

We also determined the *difference* in the fluxes between days 496 and 499 and day 670 via image subtraction. While this only

TABLE 1
MID-IR PHOTOMETRY ON DAYS 496 AND 499 AT THE POSITION OF SN 2003gd

AUTHOR/METHOD ^a	FLUX (μJy)			
	$3.6\ \mu\text{m}$	$4.5\ \mu\text{m}$	$5.8\ \mu\text{m}$	$8.0\ \mu\text{m}$
This work: PSF fit.....	19.9(3.6)	74(12)	85.5(6.5)	180(15)
This work: image subtraction.....	15.6(1.3)	72.2(2.3)	60.2(7.1)	103.2(7.7)
S06: PSF fit.....	20.8(2.6)	73.8(5.6)	64.9(7.3)	103(22)

^a This column gives the photometry method used to derive the fluxes. The “image subtraction” values were obtained by aperture photometry of subtracted images (see text). Uncertainties ($1\ \sigma$) are shown in brackets. The fluxes obtained by S06 for this epoch are shown for comparison.

gives the change in flux between the two epochs, it is a particularly powerful method of removing the effects of a spatially varying background such as is encountered in SN images from *Spitzer* (Meikle et al. 2006). Also, given the very weak flux at the SN location on day 670, this procedure provides a robust check on the net supernova emission.

For each channel, the day 670 image (PBCD processed) was subtracted from the earlier Enhanced Data Product SINGS image through the use of image matching and subtraction techniques as implemented in the ISIS 2.2 image subtraction package (Alard 2000). The $8.0\ \mu\text{m}$ subtracted image is shown in Figure 1c. In Meikle et al. (2006) we demonstrate the applicability of the image subtraction technique for *Spitzer* IRAC SN data and investigate its uncertainties. Aperture photometry of the subtracted images was then carried out using the Starlink package GAIA (Draper et al. 2002). A circular aperture of radius $2.25''$ was used for the photometry. This aperture was chosen as a compromise between maximizing the sampled fraction of source flux (the radius of the first diffraction minimum at the extreme red end of the $8.0\ \mu\text{m}$ channel is $\sim 2.6''$) and minimizing any extended residual emission in the subtracted image. Aperture corrections were derived from the IRAC PSF images available on the *Spitzer* World Wide Web site. The correction factors were 1.23, 1.26, 1.50, and 1.65 for 3.6, 4.5, 5.8, and $8.0\ \mu\text{m}$, respectively.

For each measurement, the aperture was centered on the SN image using a combination of centroid estimates and visual inspection. The residual background level was measured using a clipped mean sky estimator and a concentric sky annulus having respective inner and outer radii of 1.5 and 2.8 times the aperture radius. The results are shown in Table 1. The uncertainty was determined from the sky variance within the sky annulus. These error estimates were confirmed by measuring the variance in the (day 496 – day 499) subtracted frame for each band, assuming a similar underlying error in the unsubtracted day 670 frame, and appropriately combining the two errors. These uncertainties are quoted in Table 1. However, it is likely that additional systematic errors were present due to image-matching uncertainties.

At 3.6, 4.5, and $5.8\ \mu\text{m}$ the flux differences between the two methods all have less than $3\ \sigma$ significance (see Table 1). At $8.0\ \mu\text{m}$ the difference is over $4\ \sigma$. As discussed below, we attribute this significant difference to the presence of a residual source in the day 670 image. In Table 1 we also show the PSF-derived IRAC fluxes obtained by S06 for days 496 and 499. There is reasonable consistency with our PSF results, although at $8.0\ \mu\text{m}$ we see a higher flux at a significance of just under $3\ \sigma$. Given the complexity of the field this difference is, perhaps, not too surprising.

3.2. Days 670 and 678–681 Results

On day 670, there was no detectable source at or near the SN position at 3.6, 4.5, or $5.8\ \mu\text{m}$. However, sources were detected near the SN position at $8.0\ \mu\text{m}$ on day 670 and $24\ \mu\text{m}$ on days 678–681 (see Fig. 1). We compared the positions of these sources with that of the SN. The coordinates of the SN were measured by applying PSF fitting (using SNOOPY) to the subtracted $8\ \mu\text{m}$ image (which was in the coordinate system of the days 496 and 499 SINGS image). For this, we used the PSF obtained from the days 496 and 499 $8\ \mu\text{m}$ (SINGS) image, which has a PSF identical to that of the subtracted image. We also measured the SN coordinates in the same image using three other methods: centroiding, optimal filtering, and Gaussian fitting as implemented in the IRAF CENTER task. The mean and standard deviation of the results from these four methods were adopted as the SN position and uncertainty, respectively.

To convert the SN coordinates to the day 670 IRAC and days 678–681 MIPS images, we derived geometric transformations between these images and the days 496 and 499 $8\ \mu\text{m}$ SINGS image. The transformation between the days 496 and 499 and day 670 $8\ \mu\text{m}$ images was obtained using the centroid coordinates of 20 isolated sources visible in both frames. We used IRAF GEO-MAP to derive a general transformation including shifts, scales, and rotations in x and y , and a second-order polynomial for the nonlinear part. The transformation between the days 496 and 499 $8\ \mu\text{m}$ SINGS image and the $24\ \mu\text{m}$ MIPS image was obtained in a similar manner, using the centroid coordinates of 20 isolated sources visible in both frames.

To measure the coordinates of the 8 and $24\ \mu\text{m}$ sources detected near the SN position, we again used PSF fitting (SNOOPY). The associated uncertainties were estimated by simulating point sources using a Gaussian PSF with a flux similar to the faint source. Artificial sources were placed in each of the images at nine positions where the background was judged to have a similar level and complexity to that of the SN location. The coordinates of these sources were measured with PSF fitting using the same polynomial orders for modeling the background as for the actual 8 and $24\ \mu\text{m}$ sources. Finally, the measured coordinates were compared with the known positions of the simulated sources and the standard deviations of their offsets were adopted as the uncertainties in our coordinate measurements.

Our conclusion from the above astrometric measurements is that the $8\ \mu\text{m}$ source coincides with the SN position to within $1''$ (90% confidence), and the $24\ \mu\text{m}$ source coincides with the SN position to within $2''$ (90% confidence); i.e., in both cases the coincidence is to within 1 native pixel ($1.2''$ at $8\ \mu\text{m}$, $2.5''$ at $24\ \mu\text{m}$). The bulk of the position coincidence uncertainty arose from the PSF fitting to the days 670 and 681 sources with a smaller contribution from the coordinate transformation and a negligible contribution from measuring the position of the SN on days 496–469.

We measured the fluxes of the days 670 and 681 sources using our PSF-fitting procedure, obtaining $73 \pm 7\ \mu\text{Jy}$ at $8.0\ \mu\text{m}$ and $380 \pm 90\ \mu\text{Jy}$ at $24.0\ \mu\text{m}$. The $8.0\ \mu\text{m}$ flux is consistent with the $77 \pm 17\ \mu\text{Jy}$ difference in the flux between the days 496 and 499 image and the subtracted image (see Table 1), indicating that the difference was due to the residual source in the day 670 image. The sensitivity on day 670 and days 678–681 is dominated by the effects of the bright nearby sources on the PSF fitting. For the other three IRAC channels, upper limits were obtained based on direct PSF measurements of the day 670 images and on the difference between the days 496–499 images and subtracted images. Our $2\ \sigma$ upper limits at 3.6, 4.5, and $5.8\ \mu\text{m}$ are, respectively, 10, 20, and $35\ \mu\text{Jy}$, rounded to the nearest $5\ \mu\text{Jy}$.

3.3. Day 1264 Result

As indicated in § 2, we were recently given access to the PBCD $24\ \mu\text{m}$ MIPS image of SN 2003gd obtained within the Sugerman et al. *Spitzer* program (PID: 30494) on day 1264. Visual inspection suggests that the source near the SN position had faded since days 678–681. To investigate this more quantitatively, we subtracted the day 1264 image from the days 678–681 data using the procedures described in § 3.1.2.

We performed the subtraction on both the SINGS-processed days 678–681 image (pixel size $1.5''$) and on the two original PBCD images with the native pixel scale of $2.5''$ (an average of the native scale subtracted images was formed). A discrete source close to the SN position was observed in both subtractions. Aperture photometry of the source was carried out using a $6.1''$ radius aperture. The background was determined by using concentric

sky annuli in the ratio 1.5:2 of the aperture radius, and also by placing the aperture (without sky annuli) at a number of positions in a $2' \times 0.5'$ box centered on the SN. The uncertainty was estimated from the rms value of the aperture values in the second method. The whole procedure was then repeated with a $4.4''$ aperture radius. Generally consistent results were obtained. The mean flux measured was $295 \pm 70 \mu\text{Jy}$. We conclude that it seems likely that the days 678–681 $24 \mu\text{m}$ source faded significantly by day 1264.

4. ANALYSIS

The mid-IR fluxes for SN 2003gd on days 496–469 (Table 1) are plotted in Figure 2. The crossbars give the IRAC filter bands and the flux error bars are 1σ . We show both the PSF-derived points and those derived by image subtraction. Also shown are *BVRI* points obtained on day 493 (Hendry et al. 2005) adjusted to days 496 and 499 using the SN 1987A light curves. All the SN 2003gd points were dereddened using the Cardelli et al. (1989) extinction law with $R_V = 3.1$ and $E(B - V) = 0.135 \text{ mag}$ (Hendry et al. 2005).

There is clearly a strong mid-IR excess. The IR excess might be produced by an IR echo from circumstellar dust, but S06 argue that the decline rate is too high to be a typical IR echo. We find that it is, in fact, possible to reproduce the decline rate using a simple IR echo model (Meikle et al. 2006) with a modest dust shell, although the shell parameters have to lie within quite a narrow range. Without more extensive temporal coverage, it is not possible to conclusively eliminate a significant IR echo contribution to the mid-IR emission at days 496 and 499. However, the observed optical attenuation effects (Hendry et al. 2005; Sugerman et al. 2006) show that some dust condensation in the ejecta must have taken place. In addition, there is no sign of radio emission, implying a paucity of circumstellar matter (Van Dyk et al. 2003). Consideration of the deposited radioactive energy also tends to support dust condensation at this epoch (see below). Given these facts, plus the need for a rather specific CSM shell geometry for an IR echo to reproduce the decline rate between days 496 and 499 and day 670, we proceed on the assumption that the days 496 and 499 mid-IR flux was probably dominated by emission from newly formed dust in the ejecta.

4.1. Comparison of SN 2003gd on Days 496 and 499 with SN 1987A

In order to interpret further the days 496 and 499 mid-IR emission from SN 2003gd, ideally we would compare its spectral energy distribution (SED) with similar-epoch spectra from a sample of SNe II-P, but such a database covering the $3\text{--}9 \mu\text{m}$ range does not yet exist. The only pre-*Spitzer* $3\text{--}9 \mu\text{m}$ CCSN spectra are for SN 1987A. While SN 1987A was initially atypical (it arose from a blue supergiant star), its nebular optical/near-IR behavior has been shown (Pozzo et al. 2006) to be more similar to that of a normal SN II-P such as SN 2002hh. In addition, quite similar mid-IR spectral behavior has been found for SN 1987A and the Type II-P SNe 2004dj and 2005af around days 200–250 (Kotak et al. 2006). Only in the $[\text{Ar III}] 6.99 \mu\text{m}$ line is significantly different behavior detected. We conclude that the nebular mid-IR behavior of SN 1987A is similar to that of Type II-P events like SN 2003gd.

For comparison with SN 2003gd, we used SN 1987A spectra at $0.3\text{--}1.1 \mu\text{m}$ (SUSPECT database and Pun et al. 1995), $1.05\text{--}4.1 \mu\text{m}$ (Meikle et al. 1993), and $4.3\text{--}13.0 \mu\text{m}$ (Bouchet & Danziger 1993; Roche et al. 1993; Wooden et al. 1993). We used data from SN 1987A epochs as follows: optical/day 498, near-IR/

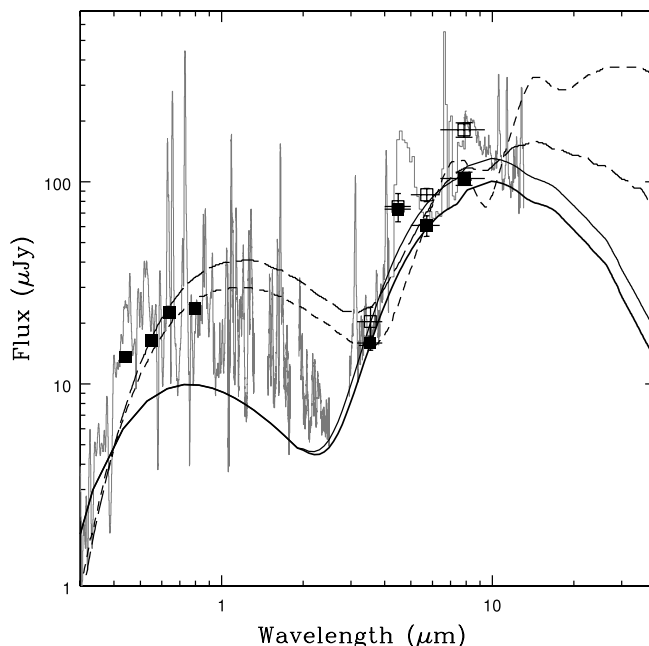


FIG. 2.— Spectral energy distribution of SN 2003gd on days 496 and 499 compared with the coeval SN 1987A spectrum and dust emission models. All data have been dereddened. The spectrum has been corrected for redshift. See text for explanation of interpolation of the data to days 496 and 499. *Open squares in IR region*: PSF-derived IRAC points. *Filled squares*: Image-subtraction-derived IRAC points. The cross bars indicate the IRAC bandwidths. *Filled squares in optical region*: Photometry from Hendry et al. (2005). *Faint structured spectrum*: Optical/IR spectrum of SN 1987A scaled to allow for differences in distance and ^{56}Ni mass. The $3\text{--}13 \mu\text{m}$ spectrum flux has been multiplied by an additional factor of 2.8. *Light solid line*: Dust emission model matched to PSF-derived fluxes at 3.6 and $5.8 \mu\text{m}$ (this work). *Heavy solid line*: Match to image-subtraction-derived fluxes at 3.6 and $5.8 \mu\text{m}$ (this work). Note that the hot component was adjusted to match the underlying continuum of the scaled SN 1987A optical spectrum and *not* the broadband points of SN 2003gd, which would contain a significant contribution from the many strong emission lines. Dust emission models from S06, *dashed lines*; smooth model, *long-dashed line*; clumped model, *short-dashed line*. [See the electronic edition of the Journal for a color version of this figure.]

day 494, mid-IR/day 494 (Meikle et al. 1993), day 517 (Roche et al. 1993), and day 518 (Bouchet & Danziger 1993). This still left the blue half of the $8.0 \mu\text{m}$ band unrepresented. To fill in this gap, which includes the strong $[\text{Ni II}] 6.63 \mu\text{m}$ line, we used the day 415 SN 1987A KAO spectrum (Wooden et al. 1993), scaled and shifted to match the days 517–518 spectra in the overlap regions ($4.5\text{--}5.3$, $7.8\text{--}12 \mu\text{m}$). All the spectra were dereddened. In addition, to convert the spectra to the SN 2003gd epochs, small scaling adjustments were made using the SN 1987A light curves. The SN 1987A spectra were then scaled by 2.9×10^{-5} and 0.21 to compensate, respectively, for the distance and ^{56}Ni mass differences between the two SNe.

Following all these adjustments, we found that the optical spectrum showed good consistency with the SN 2003gd photometry at both epochs. However, to match the SN 2003gd fluxes in the region of the IR excess ($3\text{--}13 \mu\text{m}$), we had to further increase the SN 1987A spectral fluxes by a factor of 2.0 for the image-subtracted points, and by a factor of 3.1 for the PSF-derived points. A compromise factor of 2.8 was applied (Fig. 2).

Comparison of the coeval SN 1987A IR spectrum with the days 496 and 499 SN 2003gd photometry (Fig. 2) shows that much of the IRAC fluxes are likely to be due to emission from CO ($\sim 4.8 \mu\text{m}$), SiO ($\sim 8.2 \mu\text{m}$), fine-structure lines, and $\text{Br}\alpha$. In the Kuiper Airborne Observatory (KAO) study of SN 1987A (Wooden et al. 1993), barely 20% of the fluxes corresponding to the IRAC 4.5 and $8.0 \mu\text{m}$ bands were ascribed to emission

from ejecta dust. On the other hand, in SN 2003gd the 4.5 μm point is not as far above the continuum as one might expect given the level of the SN 1987A CO emission. A similar, but less pronounced, effect may be apparent at 8 μm . This suggests that, while the factor of 2.8 scaling is appropriate to match the IR continua of SN 1987A to that of SN 2003gd, it exaggerates the line and molecular emission from the latter SN. Nevertheless, the nondust contributions to the 4.5 and 8.0 μm fluxes of SN 2003gd are probably still significant, so these points should not be used for matching any dust emission model. In contrast, the 3.6 and 5.8 μm fluxes lie quite close to the SN 1987A continuum. Given that this continuum was due to emission from ejecta dust, we conclude that these points provide a fair measure of the emission from newly formed dust in SN 2003gd. We make use of these two points in matching the dust emission model.

4.2. Dust Mass at Days 496 and 499

To estimate the dust mass produced in SN 2003gd, we compared a simple analytical IR-emission model with the observed SEDs. An additional component was added to represent continuum emission from hot, optically thick gas in the ejecta. To select the likely grain density distribution and grain materials for the dust emission model, we sought guidance from dust condensation calculations and the explosion models on which they are based. Only a few papers have been published that describe SN dust condensation based on explosion models. Such papers fall into two categories: SN 1987A, and high-redshift low-metallicity progenitor SNe. No calculations for local Type II-P events have been published. We judge the SN 1987A dust models as probably being the more relevant.

Kozasa et al. (1989) and Todini & Ferrara (2001) have calculated dust condensation within the ejecta of SN 1987A. These authors used the ejecta chemical composition as determined in nucleosynthesis models (Hashimoto et al. 1989; Nomoto et al. 1991). Both sets of authors adopted complete chemical mixing within the dust-forming zone. Within this zone, Todini & Ferrara assumed a uniform density distribution. Kozasa et al. (1989) used the density profile from an explosion model (Hashimoto et al. 1989), but this also is roughly flat. Similar dust-type abundances were obtained by both sets of authors, but neither make explicit predictions about the dust distribution within the ejecta. Recent three-dimensional CCSN explosion models (Kifonidis et al. 2006) confirm that extensive mixing of the core takes place. The same models also show that the density structure is likely to be exceedingly complex, with high-density clumps moving out through lower density gas. How this affects the dust distribution has yet to be determined.

Given the current state of knowledge, we assume that dust of uniform number density forms throughout the zone containing abundant refractory elements. The extent of this zone can be assessed using the late-time widths of metal lines. In the day 493 optical spectrum of SN 2003gd (Hendry et al. 2005), the maximum velocities implied by the metal lines generally do not exceed $\sim 2000 \text{ km s}^{-1}$. This upper limit is adopted as the size of the dust-forming region. The uniform density assumption is conservative in that it provides the least effective way of hiding dust grains in optically thick regions. Guided by the dust formation calculations (Kozasa et al. 1989; Todini & Ferrara 2001; Nozawa et al. 2003), we included silicate, amorphous carbon, and magnetite dust in the mass ratios 0.68/0.16/0.16. The mass absorption functions for the three materials were taken from the literature (Laor & Draine 1993; Rouleau & Martin 1991; Koike et al. 1981).

Our dust IR-emission model comprises a uniform sphere of isothermal dust grains. Following the escape probability formal-

TABLE 2
MODEL PARAMETERS FOR DAYS 496 AND 499

Method (1)	T_{dust} (K) (2)	$\tau_{10 \mu\text{m}}$ (3)	Dust Mass M_{\odot} (4)	f (5)	T_{hot} (K) (6)
PSF fit	525	2.6	6×10^{-5}	0.17	6700
Image subtraction.....	525	2.3	4×10^{-5}	0.13	6700

NOTES.—Col. (1) gives the photometry method used to derive the fluxes to which the model was matched. Optical depths to the center at 10 μm are shown in col. (3). The dust masses in col. (4) were derived assuming a distance of 9.3 Mpc. A 1 Mpc reduction in distance reduces the masses by about 10%. In col. (5) a “covering factor” f is shown (see text). Col. (6) gives the adopted temperature of the hot component.

ism (Osterbrock 1989; Lucy et al. 1989), the luminosity (L_{ν}) of the sphere at frequency ν is given by

$$L_{\nu} = 2\pi^2 R^2 B_{\nu}(T) \{ \tau_{\nu}^{-2} [2\tau_{\nu}^2 - 1 + (2\tau_{\nu} + 1)e^{-2\tau_{\nu}}] \}, \quad (1)$$

where R is the radius of the dust sphere at some time after the explosion, $B_{\nu}(T)$ is the Planck function at temperature T , and τ_{ν} is the optical depth to the center at frequency ν . For a grain size distribution $dn = ka^{-m}da$, where dn is the number density of grains having radius $a \rightarrow a + da$, m is typically between 2 and 4, and k is the grain number density scaling factor, it can be shown that $\tau_{\nu} = (4/3)\pi k \rho \kappa_{\nu} R [1/(4-m)] [a_{\text{max}}^{4-m} - a_{\text{min}}^{4-m}]$, where ρ and κ_{ν} are, respectively, the density and mass absorption coefficient of the grain material. The grain size distribution law was set at $m = 3.5$ (Mathis et al. 1977) with $a_{\text{min}} = 0.005 \mu\text{m}$ and $a_{\text{max}} = 0.05 \mu\text{m}$. The total mass of dust, M_d , was then found from $M_d = 4\pi R^2 \tau_{\nu} / 3\kappa_{\nu}$ (Lucy et al. 1989).

The model-free parameters are the grain temperature, sphere radius, and grain number density scaling factor, k . These were adjusted to reproduce just the 3.6 and 5.8 μm points. Wooden et al. (1993) showed that during the second year of SN 1987A, the dust-emission continuum could be contaminated by blackbody emission from hot, optically thick gas, as well as by free-bound radiation. Here we represent both effects using a single hot blackbody. The hot component was adjusted to match the underlying continuum of the scaled SN 1987A optical spectrum and *not* the broadband points of SN 2003gd, which would contain a significant contribution from the many strong emission lines. We found that the effect of the hot component on emission longward of 3 μm was small.

Model matches to both the PSF-fitting and image-subtraction-derived fluxes were obtained. The dust emission models are shown in Figure 2. We found that to achieve reasonable matches to the data it was necessary to increase the dust mass until it was optically thick in the mid-IR. Consequently, we were unable to derive a unique dust mass since, as we increase the optical depth, ever larger amounts of dust can be “hidden” with little effect on the observed radiation. We therefore, conservatively, sought the *minimum* dust mass which would provide a satisfactory match to the data. The model parameters including the derived dust masses are given in Table 2.

Dust masses of $6 \times 10^{-5} M_{\odot}$ (PSF fitting, days 496 and 499 image) and $4 \times 10^{-5} M_{\odot}$ (aperture photometry, subtracted image) were obtained. A 1 Mpc reduction in distance reduces the masses by about 10%. The uniform dust distribution of our model, optically thick at 10 μm , would surely extinguish all metal lines in the optical region. Yet, as late as day 493 (Hendry et al. 2005) and day 521 (Sugerman et al. 2006), such lines could still be seen. This implies that the dust distribution must have been “clumpy,”

allowing some of the optical line radiation to escape from the nebula. The presence of clumping is confirmed by consideration of the “covering factor,” f . This is obtained by dividing the projected area of the model dust sphere by the projected area corresponding to the estimated extent of the dust-forming zone (2000 km s^{-1}). A covering factor of ~ 0.15 was obtained (Table 2). This may also account for the relatively modest extinctions in the R band (Sugerman et al. 2006). We note that SN 1987A showed strong evidence for dust clumping (Lucy et al. 1991). In § 5 we suggest that, in general, SN ejecta dust becomes optically thick in the mid-IR when the dust mass exceeds only a few times $10^{-3} M_{\odot}$.

It is argued above that the $8 \mu\text{m}$ point should not be used for constraining the dust model due to possible contamination by SiO emission. Nevertheless, we investigated the effect of including this point and found that satisfactory matches can be obtained using somewhat lower temperatures and higher radii for the model. Similar dust masses are derived. However, the match to the SN 1987A spectrum redward of $8 \mu\text{m}$ is very poor, with the model flux exceeding the continuum flux by about a factor of 2. Given the argument in § 4.1 that the nebular behavior of SNe 1987A and 2003gd is similar, we conclude that SiO is indeed contaminating the SN 2003gd spectrum.

The total luminosity of our dust model (for the match to the PSF-derived fluxes) plus the estimated total optical/near-IR contribution (i.e., line/molecular emission plus underlying continuum) is $2.1 \times 10^{39} \text{ ergs s}^{-1}$, with roughly 30% of the luminosity arising from the dust. The ^{56}Ni mass inferred by Hendry et al. (2005) is $0.016_{-0.006}^{+0.010} M_{\odot}$. Dividing the observed total luminosity by the radioactive decay energy deposited in the ejecta (Li et al. 1993), scaled to the ^{56}Ni mass of SN 2003gd, we obtain $1.2_{-0.5}^{+0.7}$. Thus, the total luminosity is similar to that resulting from the deposited radioactive energy. This tends to support the proposition that newly condensed ejecta dust was responsible for the mid-IR continuum emission. Use of a lower distance would reduce the radioactive decay energy required to produce the observed flux. However, this would not significantly affect the energy constraints as the inferred ^{56}Ni mass would also fall—that is, the fraction of radioactive decay luminosity required to produce the observed flux would stay about the same. The dust masses we derive are about 25% of the $2.0 \times 10^{-4} M_{\odot}$, which S06 obtain from their smooth model fit at the same epoch (days 496 and 499). The S06 models are shown in Figure 2 (*dashed lines*). Between 3 and $10 \mu\text{m}$ their models are in approximate agreement with ours, but at longer wavelengths our model shows a much sharper decline. It appears that the S06 model predicts a component of colder dust and this would account for their larger dust masses. Their model invokes a source luminosity of $2.6 \times 10^{39} \text{ ergs s}^{-1}$. This is $\sim 20\%$ larger than the value in our model but is still consistent with the radioactive energy deposited, given the uncertainties in the ^{56}Ni mass.

4.3. The Days 670 and 681 Sources

S06 found a $24 \mu\text{m}$ flux on days 678–681 of $106 \pm 16 \mu\text{Jy}$. They also reported upper limits at 3.6, 4.5, 5.8, and $8.0 \mu\text{m}$ on day 670. *It is from these later epoch measurements that they deduce a dust mass of $0.02 M_{\odot}$.* As indicated above, we also obtained no detection at 3.6, 4.5, and $5.8 \mu\text{m}$ on day 670. However, at $8.0 \mu\text{m}$ we obtained a significant detection in our PSF fitting of $73 \pm 7 \mu\text{Jy}$. Moreover, inspection of Figure 1b does appear to confirm the presence of a source close to the SN position. At $24 \mu\text{m}$ our measured flux of $380 \pm 90 \mu\text{Jy}$ (see above) is about a factor of 4 larger than that obtained by S06.

To investigate this flux difference we assessed the day 678–681 MIPS sensitivity at the source position using a number of meth-

ods. The complex field in the SN vicinity makes direct noise estimation quite difficult. Therefore, to determine the underlying pixel-to-pixel noise, we subtracted the day 681 image from the day 678 image using the procedures described above. We then measured the noise at the SN location. We used a $6.1''$ radius aperture which encompasses about 0.93 of the flux in the Airy disk at $24 \mu\text{m}$. The flux in the aperture was measured at a series of locations within $40''$ of the SN position. The rms value, after aperture correction, is $\sim 200 \mu\text{Jy}$. However, as the subtracted image contained the noise of the two original images, we divided this by $\sqrt{2}$, yielding $140 \mu\text{Jy}$ as the intrinsic sensitivity (1σ) of the MIPS data. A further $\sqrt{2}$ improvement of the sensitivity to $100 \mu\text{Jy}$ arises from the fact that the SINGS-processed image, used by S06 and ourselves for the PSF fitting, is a combination of the two SINGS PBCD images.

As a further check, we examined the MIPS sensitivity in the SINGS-processed image well away from the galaxy in a relatively “clean” part of the sky, lying about $4'$ south of the SN location. Artificial stars were placed at 11 different positions within a $1' \times 3'$ area. The input star flux was set at $130 \mu\text{Jy}$ and the flux at each of the 11 positions was measured by aperture photometry, using a $6.1''$ radius aperture and a sky annulus between 1.5 and 2 times this radius. The effective sensitivity was assessed from the dispersion in the flux values. The procedure was repeated with an input star flux of $5300 \mu\text{Jy}$. The dispersion in both the low-flux and high-flux cases gave about the same result, indicating that even well away from the galaxy, the sensitivity was background limited. The 1σ sensitivity, after aperture correction, was found to be about $90 \mu\text{Jy}$, similar to the value obtained from image subtraction.

As a final check on the above procedures, we used the *Spitzer* Sensitivity-Performance Estimation Tool (PET) to estimate the intrinsic sensitivity. The measured background near the SN is about equivalent to the “high background” setting of the PET. From this we derive an intrinsic 1σ sensitivity of $60 \mu\text{Jy}$, of similar magnitude to the directly determined sensitivity values.

We conclude that the actual 1σ sensitivity of the days 678–681 MIPS image at the SN position was $\sim 90 \mu\text{Jy}$, much larger than the $16 \mu\text{Jy}$ claimed by S06. Moreover, the $106 \mu\text{Jy}$ flux at the SN position claimed by S06 would only yield a signal-to-noise ratio of about unity, not ~ 6.5 as they reported. However, we note that scaling the S06 result by a factor of 4 yields $424 \pm 64 \mu\text{Jy}$. This is more consistent with both our flux value and with our separately measured MIPS sensitivity. We suspect, therefore, that there is an error in the $24 \mu\text{m}$ flux reported by S06.

What is the origin of the 8 and $24 \mu\text{m}$ sources on days 670 and 681? Given the very crowded field within which the supernova occurred, and the fact that CCSNe tend to occur near star-forming regions, a cool background source lying close to the SN might be considered. A similar situation was described recently for *Spitzer* observations of the CCSN SN 2002hh (Meikle et al. 2006). However, the fading of the $24 \mu\text{m}$ source (§ 3.3) tends to rule out a background source, at least for most of the $24 \mu\text{m}$ flux. We shall therefore consider the implications of assuming that the sources are ultimately due to the SN.

We first hypothesize that the days 670 and 681 $8 \mu\text{m}$ and (unsubtracted) $24 \mu\text{m}$ sources have the same origin and that this origin is the SN ejecta. A simple blackbody match to our days 670 and 681 flux measurements yields a temperature of 250 K, a radius of $1.9 \times 10^{16} \text{ cm}$, and a luminosity of $9.7 \times 10^{38} \text{ ergs s}^{-1}$. This is immediately problematic. To attain a radius of $1.9 \times 10^{16} \text{ cm}$ the material at the outer limit of the blackbody would have to be traveling at 3200 km s^{-1} . This is substantially larger than the 2000 km s^{-1} limit on metal velocities indicated by late-time spectra. In addition, after adding an additional $1.1 \times 10^{38} \text{ ergs s}^{-1}$ due

to the optical/near-IR emission estimated from the optical photometry, we obtain a total luminosity of 10.8×10^{38} ergs s^{-1} . This is a factor of 4 more than the total radioactive decay energy deposited in the ejecta, according to the formula of Li et al. (1993) scaled to the ^{56}Ni mass of SN 2003gd. Indeed, it exceeds the *total* radioactive luminosity (i.e., including escaping gamma rays) by more than a factor of 2. Even allowing for the uncertainty in the ^{56}Ni mass, the energy deficit is severe. (We note that, even with their apparently underestimated $24 \mu\text{m}$ flux, the days 678–681 luminosity invoked by S06 exceeds the deposited radioactive energy by $\sim 50\%$.) It is possible for the bolometric luminosity to exceed that of the instantaneous radioactive decay deposition when the recombination timescale exceeds the radioactive or expansion timescales. However, this commences at much later epochs ($>$ day 800) than those considered here (Kozma & Fransson 1998). Thus, on both energy and velocity considerations, we have evidence that most of the 8 and $24 \mu\text{m}$ fluxes cannot be due to emission from supernova ejecta dust.

Let us now suppose that only the fading component of the $24 \mu\text{m}$ source is due to ejecta dust while the remainder of the $24 \mu\text{m}$ flux plus some or all of the $8 \mu\text{m}$ flux is due to a background source. At 250 K, to match the fading component would require a blackbody luminosity of 3 times the likely deposited radioactive luminosity and a velocity of 2800_{-400}^{+300} km s^{-1} , where the error is due to the flux uncertainty. Even if we reduce the distance by 1 Mpc and use the lower limit of the flux values, the velocity still exceeds 2000 km s^{-1} and the luminosity still exceeds the deposited radioactive luminosity by a factor of 2. Reducing the temperature from 250 to 150 K, the luminosity falls by 30% but the velocity of the blackbody surface rises to an increasingly implausible 6700_{-900}^{+700} km s^{-1} . (We note that, in their model, S06 invoke an outer limit for their dust zone of ~ 8000 km s^{-1} , which is even more unlikely.) Increasing the temperature above 250 K also does not help since the luminosity deficit problem would worsen. Moreover, this would produce an $8 \mu\text{m}$ flux in excess of that seen near the SN position. Similar results are obtained if we employ our dust emission model rather than a blackbody. We conclude that most of the fading component of the $24 \mu\text{m}$ flux cannot be due to dust in the SN ejecta.

If the mid-IR flux observed near the position of SN 2003gd is not due to condensing dust in the ejecta, then what could be the origin of the emission? The substantial fading at $24 \mu\text{m}$ between days 678–681 and day 1264 points to a causal connection with the SN. A possible scenario is that the mid-IR emission originated in an IR echo from circumstellar or interstellar gas. As an illustration, we have estimated the parameters of a dust sheet lying in front of the SN required to reproduce the fading component of the $24 \mu\text{m}$ flux. We used an IR echo model similar to that described by Meikle et al. (2006). The input bolometric light curve was based on the information given by Hendry et al. (2005) with a single grain radius of $0.07 \mu\text{m}$. Estimates were repeated using the specific grain emissivities of different dust species. Preliminary results suggest that the $24 \mu\text{m}$ flux can be reproduced with a dust sheet of H number density $\sim 10 \text{ cm}^{-3}$, gas-to-dust ratio of 100, lying 10–20 pc in front of the SN. At this distance the dust temperature is 75–90 K. The optical depth to UV-optical photons is ~ 0.2 . The echo radius would be about $0.1''$ and so such a source would be effectively coincident with the SN position. To account for the fading the dust sheet would have to be of irregular density on scales of a few parsecs (a fraction of an arcsecond). Sugerman (2005) and Van Dyk et al. (2006) found an optical echo on day 623 lying at $0.3''$ from SN 2003gd, with a strong concentration to the NW. They showed that this could be explained by a dust sheet lying about 100 pc in front of the SN. The one-sided appearance of

the optical echo suggests that such dust sheets can indeed exhibit large density fluctuations on a scale of only a few tenths of an arcsecond. We conclude that an IR echo may well be responsible for the variable component of the $24 \mu\text{m}$ flux from SN 2003gd. Further discussion of the IR echo hypothesis as applied to SN 2003gd is beyond the scope of this paper.

The key point following from the above discussion is that most of the mid-IR flux at days 670 and 681 could not have been due to dust in the supernova ejecta. In particular, it suggests that the inference by S06 of a large mass ($0.02 M_{\odot}$) of ejecta dust is unjustified.

5. CONCLUSIONS

We have examined late-time mid-IR observations of the Type II-P SN 2003gd and find the following.

1. By days 496 and 499, at least $4 \times 10^{-5} M_{\odot}$ of dust had formed in the ejecta of SN 2003gd. The larger (factor of ~ 4) mass indicated by the smooth model of S06 appears to be due to the presence of a larger component of cold dust, but this has no direct observational support. After allowing for differences in ^{56}Ni production, we find that the optical flux of SN 2003gd is similar to the coeval value for SN 1987A, while the 3–9 μm flux is almost 3 times stronger. This may indicate more efficient dust production in SN 2003gd. Nevertheless, there is no evidence at this epoch that the absolute dust production was unusually high. The dust masses and temperatures are similar to those inferred for SN 1987A (Wooden et al. 1993). There is also evidence that the dust in SN 2003gd formed in clumps. Comparison with coeval spectra of SN 1987A shows that even as late as day ~ 500 the extraction of information about dust formation from broadband photometry has to be approached with caution due to the effects of other emission mechanisms. This underlines the desirability of acquiring low-resolution spectra for such studies, since this would allow correction for forbidden lines and molecular emission.

2. Emission from pointlike sources close to the SN position was detected on day 670 at $8 \mu\text{m}$ and days 678–681 at $24 \mu\text{m}$. The fading of the $24 \mu\text{m}$ source (§ 3.3) tends to rule out a background source as the origin of the mid-IR emission, at least for most of the $24 \mu\text{m}$ flux. However, energy and velocity considerations also rule out the ejecta of SN 2003gd as the origin of most of the mid-IR fluxes. The inference by S06 of $0.02 M_{\odot}$ of ejecta dust is based on a $24 \mu\text{m}$ flux which we find is only a quarter to a third of the true value. But even if we adopt their flux, their claim of such a large mass of dust is unconvincing. The large dust mass they find appears to be a consequence of the low characteristic temperature in their model. However, in order that sufficient mid-IR radiation should escape, it seems that the dust formation zone has to be as large as ~ 8000 km s^{-1} , in conflict with the observed metal line velocities. Also, in spite of the low temperature, the input luminosity of their model required to reproduce the $24 \mu\text{m}$ flux exceeds that of the likely deposited radioactive decay luminosity. Had the correct (much larger) $24 \mu\text{m}$ flux been used, these difficulties would have been even greater. We conclude that the $0.02 M_{\odot}$ of ejecta dust deduced by S06 is unsupported by the data. These *Spitzer* observations provide no basis for the S06 claim that “the [dust] condensation efficiency implied by SN 2003gd is close to the value of 0.2 needed for SNe to account for the dust content of high-redshift galaxies.” There is, as yet, no direct evidence that CCSNe are major dust factories.

An additional argument against a large detected mass of ejecta dust in SN 2003gd is pointed out by the referee. The mass of dust inferred by S06 for SN 2003gd is a factor of 25 greater than the maximum amount in SN 1987A determined by Ercolano et al.

(2007) using a similar model. These authors suggest that this implies a much higher condensation efficiency in SN 2003gd. Yet, the diminution of the optical light curve of SN 2003gd shown in S06 about 100 days after dust formation is only about 1.3 mag, very similar to that for SN 1987A at about the same epoch after dust formation (e.g., Whitelock et al. 1989). Also the blueward shifts of the emission lines are not greater in SN 2003gd than in SN 1987A (e.g., Danziger et al. 1991). Given the apparently very different estimated dust masses between the two SNe, it is difficult to see how these observed similarities are possible. One might argue that in SN 2003gd the dust is more concentrated to the center, but this is apparently belied by the shift in the H α lines (S06) which presumably arise farther out in the envelope.

The goal of determining the true dust production in SNe via the thermal emission from the grains is very challenging. Even at wavelengths as long as 24 μm , it is likely that the dust forming in SN ejecta would become optically thick long before a universally significant mass of dust was formed. For example, consider a uniform distribution of astronomical silicate grains. For $\lambda > 20 \mu\text{m}$, $\kappa_\nu \approx 1000(\lambda(\mu\text{m})/20)^{-2}$ (Laor & Draine 1993), where κ_ν is the mass absorption coefficient ($\text{cm}^2 \text{g}^{-1}$) at frequency ν . If we set $\tau_\nu > 3$, where τ_ν is the optical depth to the dust sphere center at frequency ν , and let the radius of the refractory element zone be as large as $v = 3000 \text{ km s}^{-1}$, we obtain from our uniform dust model

$$M_d > 1.5 \times 10^{-3} [\lambda(\mu\text{m})/20]^2 [t(\text{days})/600]^2 M_\odot. \quad (2)$$

At 24 μm , and as late as 2 years after the explosion, the lower limit for the dust mass would still only be $3 \times 10^{-3} M_\odot$. Similar lower limits are obtained for other grain materials such as amorphous carbon. In general, κ_ν rises toward shorter wavelengths, producing even smaller lower limits. Dust measurement at still later epochs becomes increasingly difficult as the grains cool beyond the sensitivity limits of even *Spitzer*.

Of course, if the grains are arranged in optically thick clumps, then a large mass of dust could be hidden in the clumps. This problem has been recognized for many years, as in SN 1987A (Lucy et al. 1989; Wooden et al. 1993) and SN 1998S (Pozzo et al. 2004). Ercolano et al. (2007) have recently shown that if clumps

are optically thick in just the optical/near-IR region, but thin in the mid-IR, then the dust mass may be constrained by the observed luminosities in the two wavelength regions. However, once the dust becomes optically thick in the mid-IR it is possible to derive lower limits only. As explained above, this situation sets in when the dust mass exceeds only a few times $10^{-3} M_\odot$, well below the cosmologically interesting limit of $\sim 0.1 M_\odot$.

The value of mid-IR studies of CCSNe, such as the *Spitzer* work described here, is that they can test whether dust condensation is common in typical events (i.e., SNe II-P). This is an essential step if we are to demonstrate that CCSNe are major sources of universal dust. But if large masses of dust *are* formed in SN ejecta, the direct measurement of the total masses involved is likely to require observations at much longer wavelengths. However, even with such observations there would remain the challenge of eliminating the effects of IR echoes.

We thank the referee for valuable comments and suggestions. We are grateful to B. Sugerman and the SEEDS team for making their proprietary data available to us. We thank J. Scalo and L. Pan for helpful discussions. We also thank M. Regan for providing details about the SINGS-processed images, and B. Ercolano and M. Barlow for discussions about dust/IR emission models. S. M. was supported by funds from the Participating Organisations of EURI and the EC Sixth Framework Programme. C. L. G. was supported in part by PPARC grant PPA/G/S/2003/00040. R. K. was supported in part by EU RTN grant HPRN-CT-2002-00303. M. P. was supported by PPARC Grant PPA/G/S/2001/00512. J. C. W. and A. V. F. were supported in part by NSF grants AST 04-06740 and AST 06-07485, respectively. This work is based on observations made with the *Spitzer Space Telescope*, which is operated by the Jet Propulsion Laboratory, California Institute of Technology, under a contract with NASA. Support for this work was provided by NASA through an award (3248) issued by JPL/Caltech.

Facilities: NED, *Spitzer*, SSC Leopard Archive Tool.

APPENDIX A

SN DUST PRODUCTION REQUIRED TO ACCOUNT FOR OBSERVED HIGH-REDSHIFT DUST

Models of dust formation in CCSNe (Todini & Ferrara 2001; Nozawa et al. 2003) succeed in producing copious amounts of dust—around $0.1\text{--}1 M_\odot$ even in the low-metallicity environments of the early universe. This corresponds to a SN dust condensation efficiency of about 0.2 (Morgan & Edmunds 2003), where the efficiency is defined as the dust mass divided by the total mass of refractory elements. This is enough to account for the quantity of dust seen at high redshifts.

As a demonstration, let us consider the results of Bertoldi et al. (2003). In their study of high-redshift quasars they deduced, from the far-IR luminosities, a star formation rate of $\sim 3000 M_\odot \text{ yr}^{-1}$ and a dust formation rate of $\sim 1 M_\odot \text{ yr}^{-1}$. Consider a simple stellar mass spectrum

$$dN = \gamma M^{-2.5} dM, \quad (\text{A1})$$

where dN is the number of stars in the mass interval M to $M + dM$, γ is a constant with units of $(\text{mass})^{1.5}$, and all stars lie within the mass range $0.2 M_\odot < M < 30 M_\odot$. The total stellar mass in the interval M to $M + dM$ is given by $dM_{\text{tot}} = M dN = \gamma M^{-1.5} dM$. Integrating this equation over the stellar mass range we obtain $M_{\text{tot}} = 4.1\gamma$. In 1 yr we have $M_{\text{tot}} = 4.1\gamma = 3000 M_\odot$, so $\gamma = 732$. Stars of mass exceeding about $8 M_\odot$ will end their lives as CCSNe. Integrating equation (A1) over the range $8\text{--}30 M_\odot$, we obtain $N = 0.0381\gamma = 28.0$ —that is, about 28 CCSNe per year would occur. To produce $1 M_\odot$ of dust per year, the average dust yield of each SN would have to be $0.036 M_\odot$. Thus, the production rates of dust condensation models (Todini & Ferrara 2001; Nozawa et al. 2003) are indeed sufficient to account for the high-redshift dust.

The progenitor of SN 2003gd had a mass in the range $6\text{--}12 M_\odot$ (Van Dyk et al. 2003; Hendry et al. 2005). This would produce about $0.3 M_\odot$ of refractory elements (Woosley & Weaver 1995). Consequently, for such a SN to match the required average dust production, the refractory elements would have to be converted into dust with an efficiency of about 0.1.

REFERENCES

- Alard, C. 2000, *A&A*, 144, 363
- Arnett, W. D., Bahcall, J. N., Kirshner, R. P., & Woosley, S. E. 1989, *ARA&A*, 27, 629
- Bertoldi, F., Carilli, C. L., Cox, P., Fan, X., Strauss, M. A., Beelen, A., Omont, A., & Zylka, R. 2003, *A&A*, 406, L55
- Bouchet, P., & Danziger, I. J. 1993, *A&A*, 273, 451
- Bouchet, P., Phillips, M. M., Suntzeff, N. B., Gouiffes, C., Hanuschik, R. W., & Wooden, D. H. 1991, *A&A*, 245, 490
- Cardelli, J. A., Clayton, G. C., & Mathis, J. S. 1989, *ApJ*, 345, 245
- Cernuschi, F., Marsicano, F. R., & Codina, S. 1967, *Ann. d'Astrophys.*, 30, 1039
- Clayton, D. D., Amari, S., & Zinner, E. 1997, *Ap&SS*, 251, 355
- Danziger, I. J., Gouiffes, C., Bouchet, P., & Lucy, L. B. 1989, *IAU Circ.*, 4746, 1
- Danziger, I. J., Lucy, L. B., Bouchet, P., & Gouiffes, C. 1991, in *Supernovae*, ed. S. E. Woosley (New York: Springer), 69
- Douvion, T., Lagage, P. O., & Pantin, E. 2001, *A&A*, 369, 589
- Draper, P. W., Gray, N., & Berry, D. S. 2002, *Starlink User Note* 214.10
- Dunne, L., Eales, S., Ivison, R., Morgan, H., & Edmunds, M. 2003, *Nature*, 424, 285
- Dwek, E. 1998, *ApJ*, 501, 643
- Dwek, E., Dinerstein, H. L., Gillett, F. C., Hauser, M. G., & Rice, W. L. 1987, *ApJ*, 315, 571
- Dwek, E., Moseley, S. H., Glaccum, W., Graham, J. R., Loewenstein, R. F., Silverberg, R. F., & Smith, R. K. 1992, *ApJ*, 389, L21
- Elmhamdi, A., et al. 2003, *MNRAS*, 338, 939
- Ercolano, B., Barlow, M. J., & Sugerman, B. E. K. 2007, *MNRAS*, 375, 753
- Evans, R., & McNaught, R. 2003, *IAU Circ.*, 8150, 2
- Fall, S. M., Charlot, S., & Pei, Y. C. 1996, *ApJ*, 464, L43
- Fall, S. M., Pei, Y. C., & McMahon, R. G. 1989, *ApJ*, 341, L5
- Garnavich, P., & Bass, E. 2003, *IAU Circ.*, 8150, 3
- Gehrz, R. D. 1989, in *Proc. IAU Symp.* 135, *Interstellar Dust*, L. J. Allamandola, A. G. G. M. Tielens (Dordrecht: Kluwer), 445
- Gerardy, C. L., Fesen, R. A., Nomoto, K., Garnavich, P. M., Jha, S., Challis, P. M., Kirshner, R. P., Höflich, P., & Wheeler, J. C. 2002, *ApJ*, 575, 1007
- Hashimoto, M., Nomoto, K., & Shigeyama, T. 1989, *A&A*, 210, L5
- Hendry, M. A., et al. 2005, *MNRAS*, 359, 906
- Hoyle, F., & Wickramasinghe, N. C. 1970, *Nature*, 226, 62
- Kennicutt, R. C., Jr., et al. 2003, *PASP*, 115, 928
- Kifonidis, K., Plewa, T., Scheck, L., Janka, H.-Th., & Müller, E. 2006, *A&A*, 453, 661
- Kitaura, F. S., Janka, H.-Th., & Hillebrandt, W. 2006, *A&A*, 450, 345
- Koike, C., Hasegawa, H., Asada, N., & Hattori, T. 1981, *Ap&SS*, 79, 77
- Kotak, R., Meikle, W. P. S., Smartt, S. J., & Benn, C. 2003, *IAU Circ.*, 8152, 1
- Kotak, R., et al. 2006, *ApJ*, 651, L117
- Kozasa, T., Hasegawa, H., & Nomoto, K. 1989, *ApJ*, 344, 325
- Kozma, C., & Fransson, C. 1998, *ApJ*, 496, 946
- Krause, O., Birkmann, S. M., Rieke, G. H., Lemke, D., Klaas, U., Hines, D. C., & Gordon, K. D. 2004, *Nature*, 432, 596
- Lagage, P. O., Claret, A., Ballet, J., Boulanger, F., Césarsky, C. J., Césarsky, D., Fransson, C., & Pollock, A. 1996, *A&A*, 315, L273
- Laor, A., & Draine, B. T. 1993, *ApJ*, 402, 441
- Li, H., McCray, R., & Sunyaev, R. A. 1993, *ApJ*, 419, 824
- Lucy, L. B., Danziger, I. J., Gouiffes, C., & Bouchet, P. 1989, in *Structure and Dynamics of the Interstellar Medium*, ed. G. Tenorio-Tagle et al. (Berlin: Springer), 164
- . 1991, in *Supernovae*, ed. S. E. Woosley (New York: Springer), 82
- Mathis, J. S., Rimpl, W., & Nordsieck, K. H. 1977, *ApJ*, 217, 425
- Meikle, W. P. S., Spyromilio, J., Allen, D. A., Varani, G.-F., & Cumming, R. J. 1993, *MNRAS*, 261, 535
- Meikle, W. P. S., Spyromilio, J., Varani, G.-F., & Allen, D. A. 1989, *MNRAS*, 238, 193
- Meikle, W. P. S., et al. 2006, *ApJ*, 649, 332
- Morgan, H. L., & Edmunds, M. G. 2003, *MNRAS*, 343, 427
- Nomoto, K., Shigeyama, T., Kumagai, S., & Yamaoka, H. 1991, in *Supernovae*, ed. S. E. Woosley (New York: Springer), 176
- Nomoto, K., Sugimoto, D., & Sparks, W. M. 1982, *Nature*, 299, 803
- Nozawa, T., Kozasa, T., Umeda, H., Maeda, K., & Nomoto, K. 2003, *ApJ*, 598, 785
- Osterbrock, D. E. 1989, *Astrophysics of Gaseous Nebulae and Active Galactic Nuclei* (Mill Valley: University Science Books)
- Pei, Y. C., Fall, S. M., & Bechtold, J. 1991, *ApJ*, 378, 6
- Pettini, M., King, D. L., Smith, L. J., & Hunstead, R. W. 1997, *ApJ*, 478, 536
- Phillips, M., Navarrete, M., & Preston, G. 2003, *IAU Circ.*, 8152, 2
- Pozzo, M., Meikle, W. P. S., Fassia, A., Geballe, T., Lundqvist, P., Chugai, N. N., & Sollerman, J. 2004, *MNRAS*, 352, 457
- Pozzo, M., et al. 2006, *MNRAS*, 368, 1169
- Pun, J., et al. 1995, *ApJS*, 99, 223
- Regan, M. W., et al. 2004, *ApJS*, 154, 204
- Roche, P. F., Aitken, D. K., & Smith, C. H. 1993, *MNRAS*, 261, 522
- Rouleau, R., & Martin, P. G. 1991, *ApJ*, 377, 526
- Smartt, S. J., Maund, J. R., Hendry, M. A., Tout, C. A., Gilmore, G. F., Mattila, S., & Benn, C. R. 2004, *Science*, 303, 499
- Sugerman, B. E. K. 2005, *ApJ*, 632, L17
- Sugerman, B. E. K., et al. 2006, *Science*, 313, 196 [S06]
- Suntzeff, N. B., & Bouchet, P. 1990, *AJ*, 99, 650
- Temim, T., et al. 2006, *AJ*, 132, 1610
- Tielens, A. G. G. M. 1990, in *NASA Conf. Publ.* 3061, ed. J. C. Tarter, S. Chang, & D. J. Defrees (Washington: NASA), 59
- Todini, P., & Ferrara, A. 2001, *MNRAS*, 325, 726
- Van Dyk, S. D., Li, W., & Filippenko, A. V. 2003, *PASP*, 115, 1289
- . 2006, *PASP*, 118, 351
- Whitelock, P. A., et al. 1988, *MNRAS*, 234, 5P
- . 1989, *MNRAS*, 240, 7
- Wooden, D. H., Rank, D. M., Bregman, J. D., Witteborn, F. C., Tielens, A. G. G. M., Cohen, M., Pinto, P. A., & Axelrod, T. S. 1993, *ApJS*, 88, 477
- Woosley, S. E., & Weaver, T. A. 1995, *ApJS*, 101, 181